ELSEVIER

X-ray spectromicroscopy of immiscible polymer blends: polystyrene–poly(methyl methacrylate)

C. Morin[a], H. Ikeura-Sekiguchi[a], T. Tyliszczak[a], R. Cornelius[a], J.L. Brash[a], A.P. Hitchcock[a],*, A. Scholl[b], F. Nolting[b], G. Appel[c], D.A. Winesett[c], K. Kaznacheyev[c], H. Ade[c]

[a]*BIMR, Department of Chemistry, McMaster University, 1280 Main St. W., Hamilton, Ont., Canada L8S 4M1*
[b]*Advanced Light Source, Berkeley Laboratory, Berkeley, CA 94720, USA*
[c]*Department of Physics, North Carolina State University, Raleigh, NC 27695, USA*

Abstract

Spun cast thin films of blends of low and high molecular weight mono-disperse polystyrene (PS) and poly(methyl methacrylate) (PMMA) with nominal compositions ranging from 66/33 wt.%/wt.% (w/w) up to 10/90 w/w PS/PMMA have been studied, as-made and after annealing. Two synchrotron-based X-ray microscopies — scanning transmission X-ray microscopy (STXM) and X-ray photoemission electron microscopy (X-PEEM) — as well as several variants of atomic force microscopy (AFM) were used to probe the composition and morphology of the bulk and surface of these blends. The chemical sensitivities and spatial resolutions of these three techniques are compared. All samples are observed to have a PS signal in the C 1s X-ray absorption spectrum of the surface of the PMMA-rich domains as measured in the X-PEEM. A continuous thin PS layer is not expected at a PMMA surface since neither polymer should wet the other at thermodynamic equilibrium. The likely origin of this PS surface signal is from a bimodal distribution of PS domain sizes with the PS signal arising from domains at the surface which are smaller than the ~200-nm resolution of the X-PEEM. High resolution AFM and STXM provide direct evidence for this explanation. © 2001 Elsevier Science B.V. All rights reserved.

Keywords: Soft x-ray microscopy; NEXAFS; DS; PMMA; Polymer blends; Phase segregation; Quantitative chemical mapping

1. Introduction

Polystyrene (PS) and poly(methyl methacrylate) (PMMA) are immiscible polymers which readily phase separate in the bulk [1]. Typical annealing temperatures correspond to a deep quench into the two phase region of the phase diagram. The phases in even low molecular weight (MW) blends are nearly pure at temperatures below 200°C, e.g. PS and PMMA with MW=21K each have >99.5% pure phases at 165°C [1]. Since the interfacial tension between the polymers is larger than the difference in their surface tensions [2], it is expected that the two materials will have a strong tendency to extend the bulk phase segregation right to the surface. Indeed dewetting studies indicate that neither polymer is able to wet the other polymer [3]. PS/PMMA blends and copolymers are classic model systems for poly-

---

*Corresponding author. Tel.: +1-905-5259-1450; fax: +1-905-521-2773.
E-mail address: aph@mcmaster.ca (A.P. Hitchcock).

mer phase segregation studies, but they also have direct technological relevance. The bulk and surface immiscibility is important in nanoscale patterning. For example, thin films of PS-*b*-PMMA diblock copolymers are currently being investigated for possible use in the fabrication of high density magnetic storage media [4], while phase separated PS/PMMA blend thin films have been proposed as antireflection coatings [5]. This work was initiated as part of a biomaterials study for which we required flat, thin films of PS/PMMA blends with a surface consisting of pure PS and pure PMMA in adjacent micron-scale domains, to be used as substrates for competitive protein adsorption studies. To aid development of these substrates, we are using two types of soft X-ray microscopy, scanning transmission X-ray microscopy (STXM) and X-ray photoemission electron microscopy (X-PEEM), as well as atomic force microscopy (AFM), to investigate aspects of morphology formation and evolution in PS/PMMA polymer thin film blends. The near edge X-ray absorption fine structure (NEXAFS) [6] spectra of PS and PMMA are very different, which make this a relatively convenient polymer system to study with NEXAFS microscopy.

Heterogeneous PS/PMMA polymer thin films are typically formed from a homogeneous solution by spin casting, followed by thermal annealing. The kinetics and mechanisms of the phase separation process in the thin film; surface roughening; and the relationship between equilibrium morphology and the fabrication and materials parameters are of considerable academic and technological interest. During the initial stages of the spin casting process most of the solution is cast off leaving a thin layer on the substrate. As the layer thins due to fluid flow, the evaporation of the solvent becomes important. The effect of evaporation is to increase the concentration of the polymer in the solution. This slows the shear thinning of the film. Phase separation of the polymers can occur in the presence of the increasingly lower concentration of solvent and a wide range of initial morphologies have been observed in numerous studies of PS/PMMA thin films [3,5,7–13]. Morphologies can be produced in which one phase is encapsulated in the other with either PMMA or PS as the matrix phase, or as primarily bilayers with either PS or PMMA exposed at the surface interface. The

morphology adopted depends on the solvent, surface, and spin-casting parameters (*T*, spin rate, volume, concentration . . .) and subsequent annealing. The following bullet list itemizes and briefly describes the factors which play a role in determining the initial morphology of the as-formed film, the kinetics and mechanism of its thermal evolution, and the final equilibrium morphology.

- Molecular weight (MW) of the polymers. Differential solidification rates can lead to stratification and different matrix formation during spinning; longer chains will be less mobile and metastable structures may be more important during annealing. Above a critical molecular weight, the viscosity of polymers scales with $MW^{3.4}$ [1].
- Polydispersity ($\delta = M_w/M_n$ where M_w and M_n are the weight and number averaged MW, respectively). This has a complex influence and should be kept as close to 1 as possible (i.e. monodisperse).
- Composition ratio. In bulk materials, the majority component has a tendency to form a continuous matrix phase. In thin films, the interface and surface energies need to be considered [14].
- Substrate surface energy. This can vary dramatically depending on the substrate used and has a strong effect on morphology, especially for very thin films (<100 nm) [9]. In general one would expect vertical segregation of the components within a blend film with that component with the greater affinity for the substrate being more prevalent at the substrate interface.
- Choice of solvent. This affects evaporation characteristics and relative solubility, both of which can lead to inhomogeneous vertical or even lateral distributions of components in spun-cast polymer blend films [9].
- Temperature of substrate during spin casting. This affects solubility of polymers and the evaporation rate of solvent.
- Spinning rate. This mainly affects film thickness, although losses by preferential evaporation or solubility could be affected by rate of flow across the surface.
- Annealing procedure. Temperatures above the glass transition temperature (T_g) are required for the polymer chains to become mobile. The time

required to approach equilibrium increases at higher MW and equilibrium may never be achieved (in a human time scale at least) for sufficiently high MW systems. The kinetics of polymer phase transformations are linked to MW, film thickness, and possibly the annealing atmosphere.

• Impurities. These may act as surfactants or compatibilizers, thus changing the intrinsic phase separation processes of a given film.

PS prefers hydrophobic substrates such as H-terminated Si, whereas PMMA prefers hydrophilic substrates such as the Si–O and Si–OH terminated native oxide layer of a Si wafer (denoted SiO_x). Thus, when thin films of PS/PMMA are deposited on a Si wafer with a native oxide surface, we expect the PMMA tends to segregate to the substrate. This preference exerts its influence both during spin casting, and even more so during annealing. Tanaka et al. [8] examined PS/PMMA films up to 25 µm thick spun cast from toluene (PS: MW=90K, δ= 1.05; PMMA: MW=69K, δ=1.06) on silicon, gold and a siliconized substrate. They found considerable dependence of the phase segregation morphology and surface composition on the substrate as well as the film thickness. Walheim et al. [9] investigated PS/PMMA blends spun from toluene, tetrahydrofuran, and methyl ethyl ketone onto SiO_x, Au, and a low surface energy organic monolayer. Winesett et al. [10] have also investigated the effect of different substrates (Si, Au and Co) on PS/PMMA morphologies and their annealing behavior. In all studies, the type of substrate and solvent utilized had a pronounced effect on the as-cast morphology. For PS and PMMA, the balance of surface attractiveness can be controlled carefully and neutral surfaces can be created and selectively tuned with the use of random PS-*r*-PMMA copolymer brushes [14].

The air interface composition and morphology appear to be equally complex and might furthermore be dependent on the polymer substrate interaction in ultra thin films (<100 nm). During spin casting either polymer can separate preferentially to the air interface. This is primarily a function of the solvent and molecular weight utilized [9]. Tanaka et al. [8] reported a continuous surface layer of PS in 25-µm thick PS/PMMA films spun cast from toluene (PS:

MW=90K, δ=1.05; PMMA: MW=69K, δ=1.06), but noted that a mixed surface results for films of 100 nm or smaller thickness. Thon-That et al. [11,12] have explored the surface morphologies of PS/PMMA blend films spun cast from chloroform solution onto mica. In contrast to the observations of Tanaka et al. [8], the as-cast films studied by AFM and XPS by Thon-That et al. [11,12] have a PMMA enriched surface. On Au surfaces, Walheim et al. [9] have found PS surface enrichment for toluene and tetrahydrofuran (better solvents for PS than for PMMA), but a surface layer of PMMA for methyl-ethyl ketone, which is a poor solvent for PS. Almost a complete bilayer with PMMA on top was observed when PS/PMMA was cast from methyl-ethyl ketone on a low surface energy organic monolayer [9]. The evidence to date suggests that the surface composition of as-cast films is not so much dominated by a 'segregation' or preference of one polymer to the surface, as by the strong preference of one polymer for the substrate as well as the relative solubility of the two polymers in the chosen solvent.

During annealing, the blends should evolve towards thermodynamic equilibrium. The surface tension of pure PS and pure PMMA is almost the same. According to Wu [2], 3K PMMA and 44K PS have surface tensions of γ_{PMMA}=41.1 dyn/cm and γ_{PS}= 40.7 dyn/cm at 20°C, while γ_{PMMA}=32.0 dyn/cm and γ_{PS}=32.1 dyn/cm at 140°C. This suggests there should be very little thermodynamic driving force for surface segregation at annealing temperatures above 135°C, temperatures typically used as they are well above the glass transition temperature of both polymers (T_g(PS)~110°C, T_g(PMMA)~120°C for the MWs used [1]), yet deep within the two phase region of the phase diagram. Hence, the interfacial energy may be more important in establishing the surface morphology than the surface energies themselves, and the systems try to minimize interfacial area rather than the surface area of a particular polymer. Wu [2] calculated the interfacial tension (γ_{AB}) and spreading parameters $\{S = \gamma_B - (\gamma_A + \gamma_{AB})\}$ for PS and PMMA as a function of temperature (γ_A and γ_B are the surface free energies (surface tensions) of A and B, respectively, and γ_{AB} is the A–B interfacial energy). The interfacial tension for 44K PS and 3K PMMA [2] is 3.2 dyn/cm at 20°C and 1.7 dyn/cm at 140°C. A dewets B for a negative spreading parame-

ter. Since the interfacial tension γ_{AB} is larger than the absolute value of the surface tension difference over the entire temperature range considered ($|\gamma_{PS} - \gamma_{PMMA}| < 0.8$ dyn/cm), the spreading parameter, *S*, is negative for all annealing temperatures, irrespective of whether PS (or PMMA) is phase A or phase B. Thus neither polymer should wet the other polymer. Since γ_{AB} increases with increasing MW, *S* should be even more negative for the higher MW polymers which are typically used in many experiments.

Some experiments seem to directly confirm the implications of the spreading parameter as calculated by Wu [2]. In an investigation of a 28-nm thick PS film floated on top of a 90-nm PMMA film cast on Si, Qu et al. [3] found that PS dewets PMMA. The PMMA films were spun cast from toluene onto Si wafers and annealed at 160°C in vacuum to remove any solvent. Because various MW were used, the thickness was maintained at ~90 nm by varying the polymer concentration. The PS films were spun cast on Si, then these as-made films were floated on water, then transferred on top of the PMMA film. The bilayers were annealed at 162°C to initiate dewetting. As the annealing time was increased, increasingly larger holes formed in the PS layer.

Kumacheva et al. [15] used confocal fluorescent microscopy to study a 90:10 (w/w) PS/PMMA blend, prepared by a very slow and controlled evaporation of a 4 wt.% toluene solution (PS: MW= 234K, $\delta = 6.3$; PMMA: MW=306K, $\delta = 2.3$). This preparation, which has many factors different from those involved in spin coating, resulted in 135-nm thick PMMA lenses on top of a PMMA-depleted PS subsurface layer, and regularly distributed PMMA dispersions in a PS matrix further away from the surface.

Ade et al. [16,17] characterized films of 50:50 (w/w) PS/PMMA blends spun cast from toluene onto Si substrates with a native oxide layer (PS: MW=27K, $\delta = 1.05$; PMMA: MW=27K, $\delta = 1.10$). The 140-nm thick films were annealed at 180°C for varying times. In this case, the equilibrium system consisted of a PMMA matrix and substrate interface layer which supported PS droplets within a rim of PMMA.

In contrast to all of the above results, Thon-That et al. [11,12] concluded from angle resolved XPS data

that PS/PMMA blend films develop a PS film on top of the PMMA rich domains during annealing. The results on PS/PMMA blend films described below indicate that there are finely dispersed PS domains on top of the PMMA domains. With insufficient spatial resolution, this PS dispersion could be mistaken as a thin PS film. Other recent studies of the surface structure of polymer thin film blends include those of PS/poly(vinyl methyl ether) [18], PS/poly-(bromo-styrene) [13,19] and PS/poly(*n*-butyl methacrylate) [20]. On the silicon substrates used, PS encapsulates poly(vinyl methyl ether) [18] and poly-(bromo-styrene) [17] unless the films are too thin [13], while poly(*n*-butyl methacrylate) encapsulates PS [19].

While much of the literature is consistent, there are some apparently conflicting observations in the literature for materials which deal with the phase segregation phenomena in this or similar systems. This is probably because there are many different parameters playing a role in thin film polymer blend morphology and phase separation phenomena. Thus the actual film that results is quite dependent on the exact details of the formulation, surface composition, and annealing protocol. In order to better understand polymer blend morphology and surface properties, one needs to apply experimental techniques with good spatial resolution, high chemical sensitivity, and variable depth sensitivity to carefully selected and prepared polymer blend systems. While there are many experimental techniques to visualize morphologies of thin films of polymer blends, very few are able to provide quantitative chemical analysis at high spatial resolution, and fewer still which can examine the surface with an appropriate sampling depth. For bulk structure studies, transmission electron microscopy (TEM) has the highest spatial resolution, and in principle one can obtain chemical sensitivity through selective staining or by electron energy loss spectroscopy. However staining may introduce artefacts, and radiation damage in many polymer systems is too rapid to achieve the quality of energy loss signal needed for chemical analysis at high spatial resolution. Atomic force microscopy (AFM) is excellent for surface visualization and provides indirect chemical sensitivity through phase mode or adhesion force measurements. However it does not provide direct chemical identification and it

is extremely sensitive to the outermost layer, which in polymer systems may be unrepresentative of the relevant near-surface region due to low MW contamination. Soft X-ray spectromicroscopy (also known as NEXAFS microscopy) [21–23], in a number of variants, provides a powerful complement to TEM and AFM. In NEXAFS microscopy, inner-shell electronic excitation is used as a chemically sensitive image contrast mechanism. Scanning transmission X-ray microscopy (STXM) measures the absorption through a thin film and thus is a bulk technique. X-ray photoelectron emission microscopy (X-PEEM) measures the absorption indirectly by detecting photo-ejected electrons, and is a near-surface technique (10–15 nm estimated sampling depth). Both STXM and X-PEEM are finding increasing use in the analysis of complex polymer systems, on account of their ability to perform chemical mapping at a relevant spatial scale. In both techniques NEXAFS spectra can be acquired on a small region down to the spatial resolution limit of the instrument ('microspectroscopy'), and images can be acquired at photon energies selected for their chemical sensitivity ('analytical microscopy'). In many recent applications the full power of the combined spatial–spectral domain is exploited by automated acquisition of image sequences, which produce a three-dimensional data set which can be analyzed to extract extensive chemical information from the region studied ('spectromicroscopy'). Efficient acquisition [24] and data analysis procedures [25,26] are under active development. We refer the reader to recent reviews for full details of the rapidly growing field of soft X-ray spectromicroscopy and its applications to biology [21] and polymer science [22,23].

Here we describe some of our own recent studies on PS/PMMA thin film blends. The goal has been the preparation of samples which are fully phase segregated at the surface and which have domain sizes larger than 0.3 μm. Such samples are of interest for biomaterials-related studies of competitive protein adsorption on a surface with hydrophilic and hydrophobic domains [27]. For this we have used PMMA-rich blends made from high MW components. Some of us (Ade) had previously studied a variety of relatively low molecular weight PS/PMMA thin films with NEXAFS microscopy

techniques [16,17]. The combination of the prior low molecular weight studies and the present high molecular weight studies, carried out over a range of compositions and with various sample preparation conditions, has provided a relatively coarse sampling of the available parameter space. Although the bulk had the expected phase segregated morphology, both high MW and low MW blends were found to have a measurable PS signal in the NEXAFS spectra from regions of the presumed pure PMMA domains and, at least according to the X-PEEM results, pure PMMA could not be exposed at the surface under any of the annealing conditions employed. A main goal of this paper is to explain this initially puzzling observation, which is in apparent contradiction to the general understanding that PS on top of PMMA will dewet, and thus should consist of pure PS and PMMA domains at the surface.

To clarify some issues raised by these results, new blends prepared from low molecular weight PS and PMMA were also studied. Given the many parameters that influence morphologies in PS/PMMA thin films, perhaps it is not surprising that the various PS/PMMA polymer blends we have investigated in this study exhibit a variety of different surface and bulk morphologies. Our intent here is to use these results (i) as an illustration of X-ray microscopy as a complementary tool to AFM for studies of phase segregation phenomena in polymer thin films, and (ii) to identify the approaches which might allow preparation of fully surface differentiated PS/PMMA surfaces which we are seeking as substrates for competitive protein adsorption studies.

2. Experimental

2.1. Sample preparation

All high molecular weight polymers used for these studies were obtained from Polymer Source and used without further purification. The 66/33 (w/w) PS/PMMA sample (PS: MW=2.2M, δ=1.1; PMMA: MW=150K, δ=1.1) (w/w is wt.%/wt.%) was prepared by spin casting a 0.8% solution (total polymer in toluene). The details of the starting polymers and sample annealing are summarized in Table 1. A small volume of this solution (~50 μl)

Table 1
Details of fabrication and AFM characterization of the PS/PMMA blend samples

Sample (PS/PMMA)	PS		PMMA		Spin casting (%)[a]	Vacuum anneal	Thickness (nm)[b]	rms Surface roughness (nm)
	MW	δ	MW	δ				
66/33	2.2M	<1.1	150K	<1.1	0.8	120°C, 55 h	32 (SiO$_x$)	4.5
40/60	21K	1.02	22K	1.03	1.4	165°C, 24 h	50	–
50/50	27K	1.02	27K	1.03	1.4	180°C, 1 h	60	12
30/70	1.06M	1.06	312K	1.01	1	140°C, 2 h	61 (SiO$_x$)	4
							82 (Si$_3$N$_4$)	6
10/90	1.06M	1.06	312K	1.01	1	180°C, 30 min	5.8 (SiO$_x$)	3.2

[a] All spin casting was done from toluene solutions of the indicated total wt.% polymer.
[b] Measured by AFM from height between the polymer surface and the bottom of an adjacent scratch, which exposed the substrate.

was passed through a teflon micropore filter to remove particulate impurities and dropped onto the spinning substrate at 4000 rpm. Spinning was continued for ~5 s. The 66/33 samples were vacuum annealed at 120°C for 55 h then cooled to 40°C over a period of 5 h. The 10/90 (on Si) and 30/70 PS/PMMA samples were made from a different set of polymers (PS: MW=1.07M, δ=1.06; PMMA: MW=312K, δ=1.01). Thin films of the 10/90 and 30/70 samples were spun cast from toluene (1% by weight solution) onto native oxide Si (for X-PEEM) and gold-coated Si$_3$N$_4$ membranes (for STXM). The 10/90 sample was vacuum annealed at 180°C for 2 h then cooled to 30°C over 8.5 h. The 30/70 samples were vacuum annealed at 140°C for 2 h, followed by slow cooling over 12 h. During annealing the samples were pumped continuously using an untrapped diffusion pump with silicone fluid. The samples were transferred to the microscope in air, in a protected enclosure.

The low molecular weight 40/60 w/w PS/PMMA samples were prepared by spin coating from toluene (1.4% solution) (PS: MW=21K, δ=1.02; PMMA: MW=22.65K, δ=1.03; Polymer Laboratories) on SiO$_x$ and annealing at 165°C for 24 h in a vacuum oven (<10^{-4} Torr), followed by a sudden quench to room temperature. For STXM investigations the low MW films were floated from the silicon substrate and mounted on TEM grids.

2.2. X-PEEM and STXM

Scanning transmission X-ray microscopy (STXM) was performed at beamline 7.0.1 of the Advanced Light Source (ALS) [28] and at the Stony Brook

instrument on X1A at the National Synchrotron Light Source (NSLS) [29–31]. The STXM optical layout is depicted in Fig. 1a. In STXM, a Fresnel zone plate (ZP) is used to focus monochromatic X-rays (ΔE ~0.15 eV) to a small spot, which is 50 nm if the ZP is operated at the diffraction limit (coherent illumination). Images are acquired by raster scanning an X-ray translucent sample in the focal spot while detecting the flux of transmitted X-rays. The sample is in a He atmosphere. Spectra are obtained by successively stepping the X-ray energy through a spectral region while recording point, line, or image data. In the ALS studies, image sequences[1] have been used to provide detailed chemical mapping. At the NSLS, high resolution images at chemically sensitive energies were obtained. Fig. 1b plots the C 1s spectra of PS and PMMA on a quantitative linear absorption scale. These spectra were extracted from ALS STXM image sequences recorded on the 30/70 PS/PMMA sample (PS taken from the as-made, and PMMA taken from the annealed data set). The vertical scale was derived by normalization to computed linear absorption coefficients for PS and PMMA outside of the structured NEXAFS region, using the tabulated elemental X-ray absorption response [32] and the known bulk densities (PS=1.05 g/cm^3, PMMA=1.19 g/cm^3 [33]). For each species, prior to conversion to the quantitative linear absorption scale, a fraction of the other component has been subtracted since all regions of the bulk have some PS and some PMMA (the raw and subtracted

---

[1]Examples of the STXM and X-PEEM image sequences for the annealed 30/70 sample have been deposited as supplementary material with the journal (WEB ACCESS details).
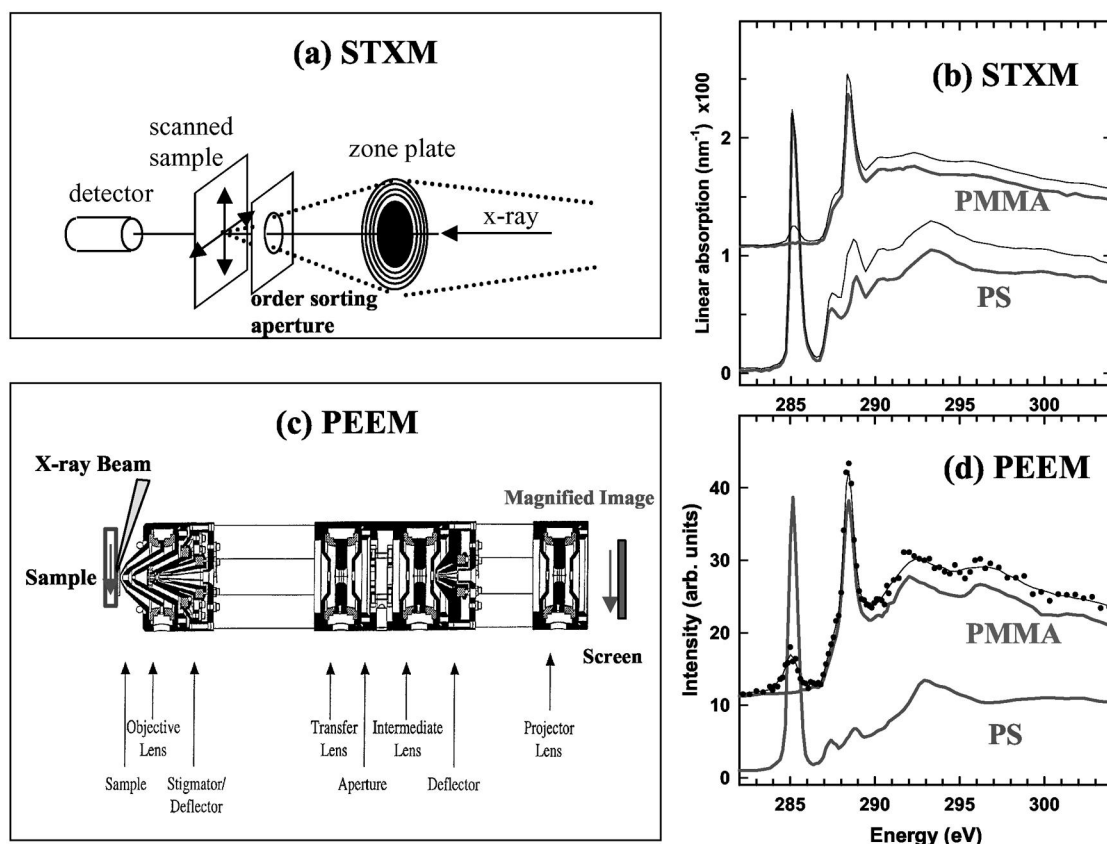
Fig. 1. (a) STXM optics. (b) C 1s NEXAFS spectra of PMMA and PS derived from STXM image sequences. The as-recorded spectra are indicated by the thin lines, while the estimated pure material response are the thick lines (see text). The measured OD intensities have been converted to linear absorption coefficient by normalization below 284 and above 300 eV to the linear absorption for pure PS and PMMA computed from elemental absorption parameters [32] and the known densities. (c) ALS X-PEEM optics. (d) C 1s NEXAFS spectra of PS and PMMA derived from X-PEEM image sequences. A portion of the PS signal has been subtracted from the PMMA signal to reduce the intensity of the 285-nm signal to baseline. In (b) and (d) the PMMA spectrum has been offset by 1 and 10 units, respectively.

spectra are shown in Fig. 1b). The amount removed was selected by requiring the resulting spectrum to have a shape similar to the spectra of pure PS and PMMA recorded with the NSLS STXM. In order to have the same energy point sampling and spectral resolution, we prefer to use the reference data taken from the same instrument as that used for a given study, even though these corrections are needed. The signal contrast in STXM arises exclusively from the X-ray absorption coefficient and the transmission signal, after conversion to optical density, provides accurate quantitation [22,23].

Surface sensitive X-ray microscopy was performed at the photoelectron emission microscope

(X-PEEM) on ALS beamline 7.3.1 [34]. The X-PEEM optical layout is depicted in Fig. 1c. Here, a 300×30-μm spot impinges the sample surface at a 30° incident angle and the photo-ejected electron distribution is imaged using an electrostatic column. Polymer samples for X-PEEM must be ultra high vacuum compatible, flat, and sufficiently thin to provide enough conductivity to avoid extensive charging. The C 1s spectra of PS and PMMA extracted from X-PEEM image sequences recorded on the as-prepared 30/70 PS/PMMA sample are plotted in Fig. 1d. The PS spectrum is the as-recorded signal taken from regions where there is only PS in the sampling depth of the X-PEEM.

Because of the ubiquitous surface PS signal, a small amount of the PS spectrum has been subtracted from the as-recorded PMMA signal to get the PMMA reference spectrum used in further analyses. The raw data, and thus the amount of PS in this optimal PMMA region, is indicated in Fig. 1d. In contrast to STXM, the signal in X-PEEM is determined not only by X-ray absorption, but also by many other factors — topography, shadowing, work function, and charging. As a consequence, procedures for quantitative chemical analysis are much less developed for X-PEEM than for STXM. The vertical scales of the X-PEEM reference spectra are set by adjusting the difference in intensity at 308 and 280 eV to an arbitrary value of 10.

3. Results

3.1. High molecular weight PS/PMMA thin films

3.1.1. Bulk versus surface morphology

Although we present in detail only the results for 30/70 blends made from the high MW components,

similar results (not shown here) have been obtained for 90/10 and 66/33 PS/PMMA blends. For STXM the PS/PMMA blend was spun cast on a Au-coated X-ray transparent silicon nitride window, whereas for X-PEEM the substrate was a Si wafer, without removal of native oxide. Thus the surfaces relevant to preferential adhesion of the two components were SiO_x in the case of X-PEEM, and Au, in the case of STXM. From other work [8,10], it is known that SiO_x has a lower water contact angle than Au and thus it would be expected that the attraction for PMMA would be greater for the SiO_x surface that the Au surface. Other than the different substrate, the details of preparation of the STXM and X-PEEM samples are identical (solution composition, spin casting, annealing procedures). AFM was recorded from each type of sample.

Fig. 2 plots STXM and X-PEEM images of the annealed 30/70 PS/PMMA recorded at the $\pi^*_{C=C}$ transition in PS (285.1 eV), the $\pi^*_{C=O}$ transition in PMMA (288.4 eV), and in the C 1s continuum (300 eV). A common grey scale for these images (0–1.4 OD for STXM, 0–110 arbitrary units for X-PEEM) is used so that the image intensity reflects the actual
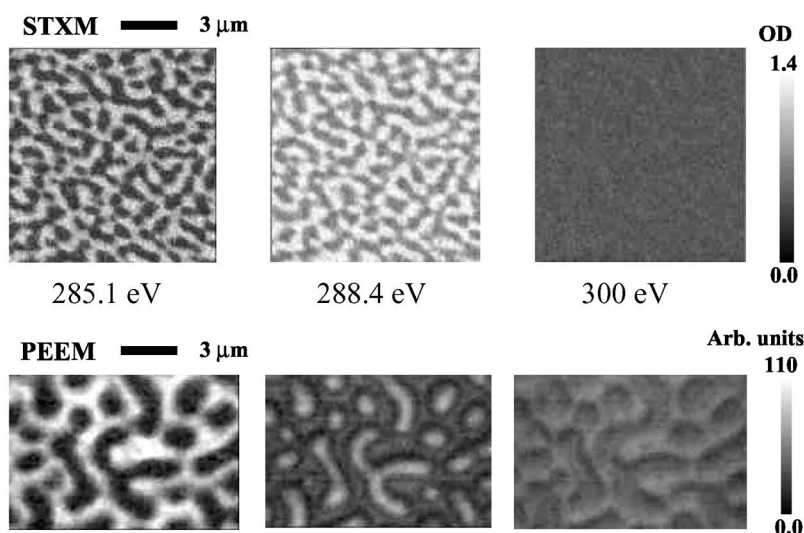

Fig. 2. STXM (upper) and X-PEEM (lower) images of annealed 30/70 (w/w) PS/PMMA recorded at 285.1, 288.4 and 300 eV. The images are presented on the same spatial scale. The sample for STXM was spun cast on Au-coated silicon nitride, while that for X-PEEM was spun cast on an oxidized silicon wafer. The STXM images are displayed in optical density using a common gray scale (B=0, W=1.4 OD units). The X-PEEM images have been normalized to incident flux (recorded independently from an HF-etched Si wafer) and are plotted on a common gray scale (B=0, W=110 arbitrary intensity units). In each case lighter pixels indicate stronger X-ray absorption (and/or, in case of X-PEEM, higher probability of electron emission). (ALS X-PEEM, ALS STXM).

signal level at each pixel at each energy. The spatial scale is identical in each of the images displayed in Fig. 2. The apparently finer scale of the microstructure in the STXM may reflect contributions of domains at different depths through the ~80-nm thin film. The sensitivity to the chemical identity through the complete contrast reversal between 285.1 and 288.4 eV is very clear. The PS domains are those regions which are bright at 285.1 eV and dark at 288.4 eV. The absence of contrast in the STXM image at 300 eV provides a useful constraint on the film structure. From atomic X-ray absorption factors [32], it is known that PS has ~60% larger optical density (OD) than PMMA at 300 eV (OD(PS)/OD(PMMA) = 1.62 at 300 eV). Even for the annealed sample the PS and PMMA domains do not appear to extend completely through the film so each pixel has some admixture of PS and PMMA. Thus, in order for the contrast to disappear at 300 eV the difference in linear absorption coefficients has to be compensated by differences in the relative amounts of PMMA and PS.

Like the STXM results, the X-PEEM images at 285.1 and 288.4 eV have reversed contrast, clearly identifying the domains. The contrast at 288.4 eV is lower than that at 285.1 eV in both STXM and X-PEEM, since PS has strong absorption whereas PMMA has negligible absorption at 285.1 eV, while both PS and PMMA absorb at 288.4 eV. In contrast to STXM, the X-PEEM image at 300 eV has the same pattern as that at 285.1 eV (PS domains strong), although of lower contrast. The residual contrast in the X-PEEM image at 300 eV is notable, and again places important constraints on the film structure within the near surface region sampled. Another notable feature of the X-PEEM results is the existence of a shading at the boundaries of the light features in the 288.4- and 300-eV images which is absent in the 285-nm image. This may arise from sample topography in which case it would reflect an altered efficiency of electron collection from a sloped surface. However, the angle is actually rather shallow: from the AFM studies of this surface, the difference between high and low regions is only 10–20 nm, while the domains are more than 1 μm in size. Also, one would expect a topography derived signal to contribute at all photon energies. A more plausible origin is a contaminant which partially

segregates to the PS-PMMA interface. Two possibilities are siloxane (ubiquitous) or silicone (diffusion pump oil from the vacuum annealing). The detailed analysis of the NEXAFS spectrum from the shadow region is consistent with the presence of ~20% contamination in the surface region sampled by X-PEEM. A similar signal is also detectable at a few percent in the bulk STXM results (vide infra). The component maps for this contaminant signal indicate that it occurs over the whole surface, with greater amounts at the interfaces between the PS-rich and PMMA-rich domains. While clearly we would prefer to have uncontaminated samples (and are revising procedures to achieve this), the detection and mapping of this signal is a good example of how NEXAFS microscopy can probe sample details missed by chemically insensitive probes such as AFM.

Maps of the PS and PMMA bulk and surface domains were obtained by recording and analysing image sequences in both STXM and X-PEEM. Analysis using all of the images allows the full spectral variation to be used in deriving quantitative spatial distributions (maps) of the PS and PMMA components. A pixel-by-pixel linear regression procedure [26] was used to derive the component maps presented in the remainder of this manuscript. For STXM, where quantitative reference standards exist, this analysis provided a quantitative picture of the film structure. For X-PEEM, only a semi-quantitative picture of the near surface region is obtained.

Fig. 3 compares component maps derived from X-PEEM and STXM with AFM images for the annealed 30/70 PS/PMMA sample. Fig. 4 presents the PS and PMMA maps in comparison to AFM for the as-made 30/70 PS/PMMA sample. In each case, two height-mode AFM images are displayed, to check for sensitivity of the surface morphology to the type of substrate used. On both SiO_x and Au/Si_3N_4 substrates the continuous phase in the AFM image has slightly larger area. The relative amounts, and the continuity, would suggest that the majority PMMA component is the continuous phase. In Figs. 3 and 4 the chemical analysis derived from the X-PEEM and STXM image sequences is presented as a single color-coded composite map while the maps of the individual PS and PMMA components of the annealed 30/70 PS/PMMA are presented in
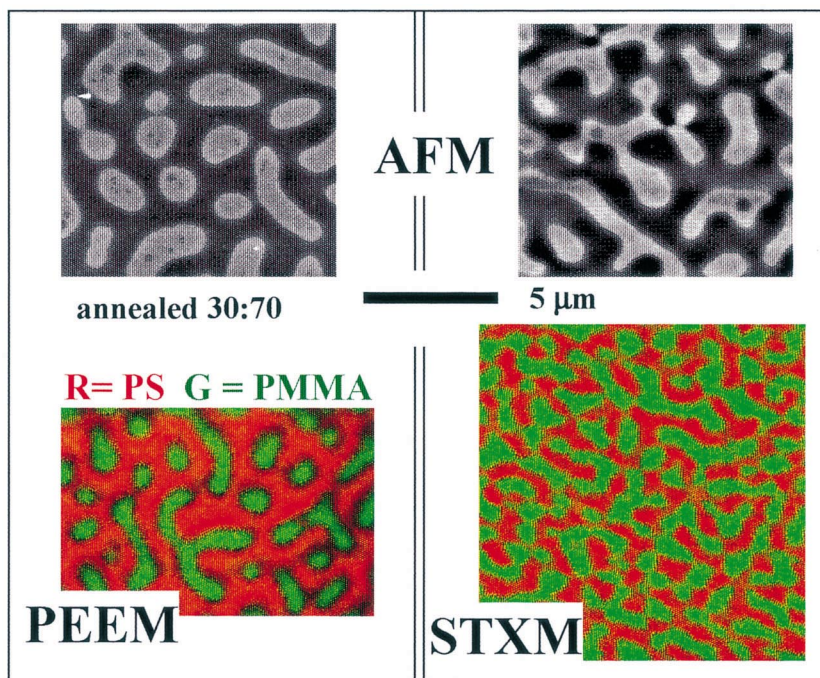
Fig. 3. Comparison of AFM, X-PEEM and STXM results for annealed 30/70 (w/w) PS/PMMA. The STXM was measured from a film spun cast on a Au-coated silicon nitride window, whereas the AFM and X-PEEM were recorded from the blend spun cast on a Si wafer covered with native oxide. The AFM height-mode images located above each X-ray micrograph are for samples prepared on the same substrate as the corresponding X-ray micrograph. Ex-situ vacuum annealing was carried out as indicated in Table 1. The X-PEEM and STXM are color coded composite images derived from the individual PS and PMMA component maps obtained by linear regression analysis of the C 1s spectrum at each pixel (Figs. 5 and 6). The color intensities in STXM are independently scaled to better represent spatial relationship, although at the cost of relative intensities. A third, impurity component was not included in this composite (see spectral fits in Figs. 7 and 8). The thickness of the sample was ~60 nm as determined by AFM from the step height at a scratch. (McMaster AFM, ALS X-PEEM, ALS STXM).

Fig. 5 for X-PEEM and in Fig. 6 for the STXM results. For both the annealed and as-made samples, the X-PEEM result clearly indicates that the continuous phase is predominantly PS. Thus X-ray microscopy shows immediately that a simplistic interpretation of the AFM — namely that the continuous phase is the majority PMMA species — is incorrect. In contrast to X-PEEM, the STXM images shows phases that are about equally continuous, with perhaps a small preference for PMMA domains to be encapsulated by PS domains. The value of the direct chemical sensitivity of NEXAFS microscopy to clarify the interpretation of AFM is well illustrated by this example. This has been noted in earlier comparisons of AFM and NEXAFS microscopy of polymers [13,17,19,20].

Table 2 summarizes the quantitative analysis of the surface and bulk composition of the as-made and annealed 30/70 blend. X-PEEM indicates that in each case, ~2/3 of the surface is PS-rich while 1/3 of the surface is PMMA-rich, based on pixel counting, using a threshold of ~50% of full range intensity in each component map. This is consistent with the AFM which indicates ~60% of the surface is the continuous, PS domain. It is clear that the surface region of these samples is highly enriched in PS relative to the 30/70 w/w starting composition (note that a wt.%/wt.% of 30/70 corresponds to a mol.%/mol.% composition of 29/71 (mol/mol) and a vol.%/vol.% composition of 33/67 (v/v) so the units used to express the composition do not play a significant role in this system). In contrast, the
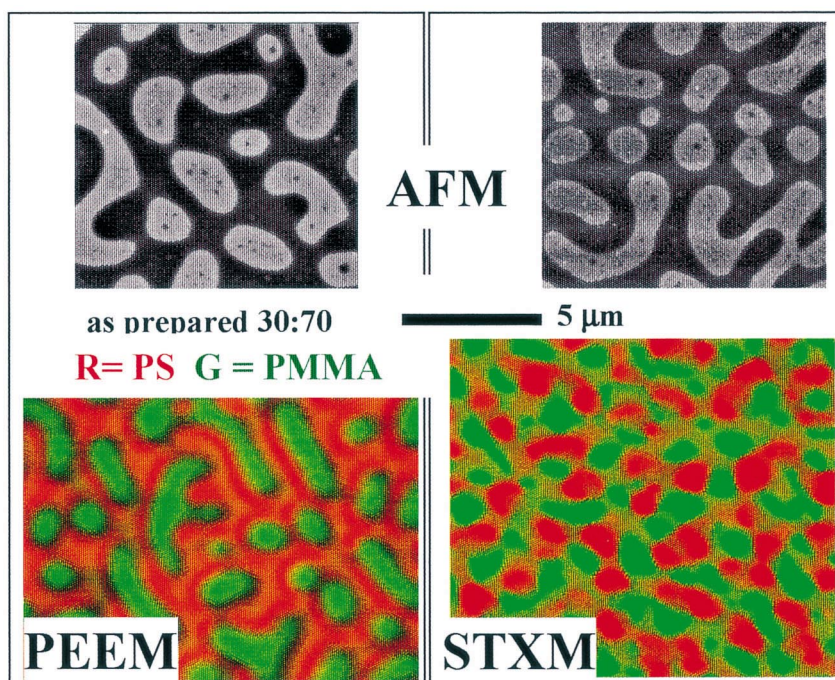
Fig. 4. Comparison of AFM, X-PEEM and STXM results for as-prepared 30/70 (w/w) PS/PMMA. Details as indicated in the caption of Fig. 3. (McMaster AFM, ALS X-PEEM, ALS STXM).

STXM analysis indicates a composition of 28(4)/72(4) PS/PMMA for the annealed sample, and 24(3)/76(4) PS/PMMA for the as-made sample. Both values are in good agreement with the starting composition suggesting that differential solubility did not modify the polymer composition through preferential loss in the spin cast process (only a small portion of the drop deposited forms the actual thin film, most of the polymer is flung off the substrate). The STXM quantitation is based on the average thickness of each domain type in the maps generated using the OD models. Both the X-PEEM — STXM comparison (Fig. 3), and the quantitative analysis of the annealed sample, indicate that, even after annealing, the surface structure does NOT extend through the full film but rather reflects some mechanism leading to an enrichment in PS at the surface of this sample. This could arise from depletion of PMMA due to a PMMA wetting layer on a SiO_x surface, repeatedly observed in prior studies, that would enrich the surface in PS. Alternatively there could be

PS surface segregation as suggested by some [8,9]. A third possibility could be that the surface structure is the result of a kinetic factor and incomplete annealing.

The surface morphology of the as-prepared 30/70 PS/PMMA as revealed by AFM and X-PEEM is rather similar to that of the annealed sample (compare Figs. 3 and 4). In contrast, the STXM chemical map of the as-prepared 30/70 sample is qualitatively very different from that of the annealed sample. In particular, there are three main intensity levels in the STXM of the as-made sample. The bright regions are columns of mainly PS, the dark areas are columns of mainly PMMA, and the intermediate grey level indicates regions in the sample where both PS and PMMA are present in the column being sampled. Variable angle STXM tomography [35] would be required to determine unambiguously the three-dimensional relationship among the domains. Another difference is the presence in the as-prepared sample of many small domains of PS embedded in the
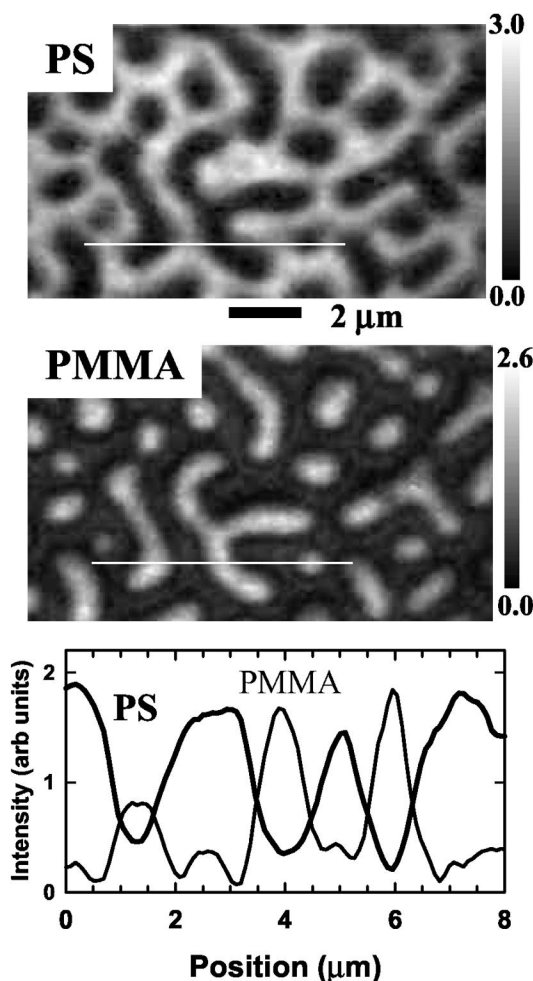
Fig. 5. PS and PMMA component maps derived from X-PEEM for annealed 30/70 (wt.%/wt.%) PS/PMMA. The vertical scales are in units of normalized response derived by setting the 300–282-nm intensity jump in the PS and PMMA reference spectra to 10. The lower plot is the intensity profile along the line indicated in the component maps. Note that the PMMA signal goes close to zero in the PS-rich regions but the PS-signal always is offset from zero. (ALS X-PEEM).

Fig. 6. PS and PMMA component maps derived from STXM for annealed 30/70 (w/w) PS/PMMA. The vertical scales are thickness in nm, derived by using the PS and PMMA reference spectra calibrated in linear absorption coefficient. The lower plot is the intensity profile along the line indicated in the component maps. (ALS X-STXM).

PMMA domains. In the AFM height mode image of the as-made sample, the PMMA domains (white) contain a large number of holes (likely small PS domains), which are absent in the AFM image of the annealed sample. Larger examples (>100 nm) of these embedded PS domains can be seen when the X-PEEM data is examined carefully. In the AFM

height image of the annealed 30/70 PS/PMMA sample (Fig. 3) there are some larger PS domains which appear to be coalesced versions of the smaller domains. In some cases shading in the AFM height image suggests these 'enclosed' PS domains lie below the surface.

Table 2
Composition of as-prepared and annealed bulk and surface of 30/70 PS/PMMA films as determined by STXM, X-PEEM and AFM

Sample	Anneal	STXM (vol.%/vol.%)[a]	X-PEEM (area/area)[b]	AFM (area/area)[b]
30/70 on Au	N	24(3)/76(4)	–	50/50
30/70 on Au	Y	28(4)/72(4)	–	60/40
30/70 on SiO$_x$	N	–	62(5)/38(5)	56/44
30/70 on SiO$_x$	Y	–	62(5)/38(5)	60/40

[a] Based on the average thickness of component maps for the same area.

[b] Based on thresholding at a level that separates the X-PEEM or AFM maps into the two dominant domains, then counting pixels.

3.1.2. Surface composition analysis: origin of PS in PMMA domains

When the NEXAFS spectrum of PMMA-rich regions is extracted from X-PEEM image sequence data for the annealed 30/70 sample, a peak is invariably observed at 285 eV, suggesting there is PS in the surface (and possibly bulk) of the PMMA domains in the film. An example of this is presented in Fig. 7 which plots the average NEXAFS spectrum at selected pixels in PS-rich and PMMA-rich domains of the X-PEEM image, along with a spectral decomposition of the extracted spectra into PS and PMMA components. Assuming no work function effects, the spectral decomposition indicates ~12% of the NEXAFS signal comes from PS in the PMMA region. Note that the sampling depth in X-PEEM is sample dependent (due to different work functions and bulk electron transport properties), but probably of the order of 10–15 nm. Fig. 8 presents the C 1s spectra of the bulk of the PMMA domains of the annealed 30/70 PS/PMMA sample as measured by STXM. Relative to that found in the X-PEEM, there is less 285-eV signal in the STXM data and the shape is less well defined, suggesting possible impurity contributions, as well as some PS. Assuming all the 285-eV signal arises from PS, the amount (~7%) would be equivalent to a uniform ~5-nm thickness of PS over the PMMA domains, or to non-uniform PS domains with 7% volume fraction. The latter is consistent with unresolved small droplets of PS distributed throughout the PMMA domains. Note the ~80-nm film thickness determined from STXM quantitation is in good agreement with that of 80 nm measured by AFM from the jump at a scratch (see Table 1). A uniform thin layer of PS at the surface would give a strongly enhanced signal in the X-PEEM relative to that seen in STXM, on account of the exponential decay of X-PEEM signals with sampling depth. Even if the sampling depth was 15 nm, a 5-nm thick PS surface layer would result in a much larger PS signal than that found in the X-PEEM analysis (Fig. 7). Since the as-cast film is very far from equilibrium and the high molecular weight PS used in the 30/70 sample can diffuse only slowly during the relatively shallow and short anneal, it is possible that a temporary PS enriched surface gradient layer develops as the PS moves to get out of the PMMA domains. Alternatively, on account of slow diffusion rates, and random break-up of PS domains, it is possible the PMMA domains could end up enclosing small, pure PS droplets.

Based on the STXM/PEEM quantitation and the AFM studies presented below, we believe that the 285-eV signal arises from very small PS domains in the PMMA domains. The size of these domains must be smaller than can be resolved by either X-PEEM (~200-nm spatial resolution) or STXM (~90-nm spatial resolution) but should be observable with AFM (~5 nm). Indeed, the AFM of the as-prepared 30/70 sample shows PS domains below 100 nm with a frequency corresponding to ~20% of the area of the large PMMA domain (Fig. 3), providing support for this interpretation. However these domains are less frequent in the AFM of the annealed 30/70 sample (Fig. 3), somewhat inconsistent with the observation of similar amounts of 285-eV signal in PMMA domains in X-PEEM of both the annealed and as-made samples. If the PS signal in the PMMA domains persists throughout the whole film, then one would expect the PS signal in PMMA domains to be
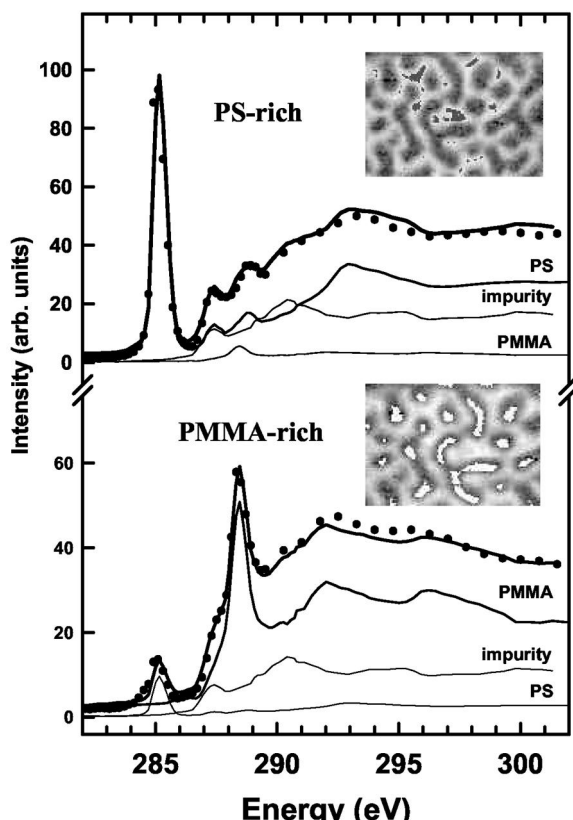
Fig. 7. Spectral decomposition of the C 1s spectra extracted from the PS-rich (2.5*PS, 1.5*impurity, 0.2*PMMA, where the reference spectra are jump-normalized) and PMMA-rich (0.25*PS, 1.0*impurity, 1.8*PMMA) domains of the near surface region of annealed 30/70 PS/PMMA measured by X-PEEM. The pixels contributing to the spectra are indicated in the insert images. In addition to a significant PS component in the PMMA domains and a small but detectible PMMA signal in the PS domains, the fit to the NEXAFS spectra indicates there is a third component ('impurity') at the surface with an aliphatic character. This could be a surface contaminant such as a siloxane or silicone from the preparation. (ALS X-PEEM).
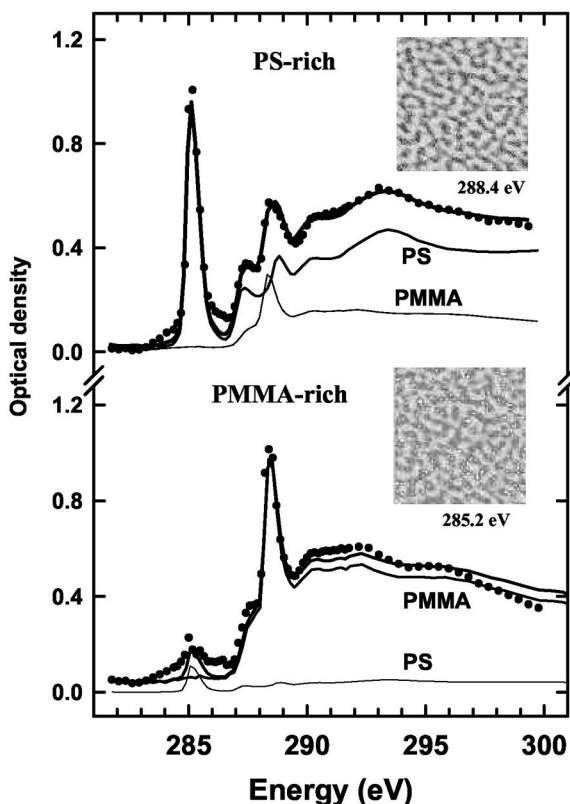

Fig. 8. Spectral decomposition of the C 1s spectra extracted from the PMMA-rich (45 nm PS, 22 nm PMMA) and PS-rich (5 nm PS, 72 nm PMMA) domains of the annealed 30/70 PS/PMMA measured by STXM. The component thicknesses were derived by extracting the sum of the spectra at the indicated pixels (black on upper image, and white on lower image) and fitting to the linear absorption coefficient reference spectra for pure PS and PMMA. The spectra could be fit satisfactorily using only the PS and PMMA components. (ALS STXM).

of similar intensity in STXM and X-PEEM. The analysis of the NEXAFS spectra of PMMA domains in the annealed sample recorded by STXM shows that the PS signal averaged throughout the whole thickness of the PMMA domains is similar but somewhat smaller than at the surface, a maximum of 7% by STXM versus 12% by X-PEEM of PS in the PMMA domain spectrum (Figs. 7 and 8). Thus it is

difficult to say on the evidence at hand if the PS droplets in PMMA domains are uniformly distributed or preferentially in the near surface region.

Two other structural models were considered, but are considered unlikely. One possible explanation is localized subsurface PS. Since the principal domains are very large laterally (1–3 μm), such domains would have to be very sheet-like for the observed PS signal to arise from a PS domain fortuitously underlying a PMMA domain. It seems rather implausible

that such a sheet-like domain would occur at about the same shallow depth below each PMMA domain. A second possible explanation could be the existence of a film of PS over the whole surface. This was the interpretation proposed by Tanaka et al. [8] for films much thicker than examined here. However, as outlined in the introduction, this contradicts the known thermodynamics for this system. Thus it could only exist if the system is far from equilibrium and a surface enriched PS layer formed as a consequence of the kinetics of the film formation and was maintained because there was insufficient annealing. Annealing clearly changes the bulk morphology of the 30/70 PS/PMMA blend (compare the STXM maps in Figs. 3 and 4) as well as the surface (see the AFM in Figs 3 and 4). This is inconsistent with a metastable surface PS layer.

Two alternative explanations of the 285-eV signal detected in the PMMA-rich domains relate to instrumental details of the X-PEEM. While possible, we do not believe they are the correct explanation. At full intensity, the X-PEEM beam line at ALS has a rather high flux ($\sim 10^{11}$ ph/s in the spot on the sample at the C 1s edge) and thus one possible explanation is that the 285-eV signal is not from PS but rather from the products of radiation damage of PMMA [36]. Radiation damage of PMMA leads to loss of the pendant methyl ester with associated reduction in the 288.4 eV $\pi^*_{C=O}$ signal and mass loss. The photoejected electrons can also reduce the saturated backbone to form C=C bonds which would produce signal at 285 eV. Studies of pure PMMA were carried out to understand these effects and identify operational regions where the damage is minimal. In order to rule out the possibility that the 285-eV signal corresponds to a damage product, we also measured the 30/70 PS/PMMA sample as a function of radiation dose, using for each dose a fresh sample area. At high doses the 288.4 eV $\pi^*_{C=O}$ signal is reduced with increasing dose while the 285-nm signal increases, although more slowly. Based on these damage rate studies, we are confident that for all except the data shown in Fig. 11, the dose used was sufficiently low to ensure the 285-eV signal introduced by damage was negligible. Thus we conclude that the 285-nm signal observed in the low dose measurements reported herein is NOT from

radiation damage but rather reflects the original chemistry of the sample.

A second possible instrumental artefact is limited spatial resolution. If the point spread sampling function [30] of the X-PEEM electron optics has low level wings then the 285-eV signal observed at the location of PMMA domains could arise from adjacent PS domains. For this to occur, the spatial sampling would have to extend several microns. Measurements of the point spread function of the X-PEEM using a very sharp, high contrast object indicate the wings extend only a few hundred nanometers from the point sampled under the electron optical conditions employed. There is an intermediate aperture in the X-PEEM (Fig. 1) which controls spatial resolution by restricting the angular sampling of the optical column. Smaller apertures reduce the wings of the point spread function at the expense of signal intensity. We have ruled out this explanation by measuring fresh regions with 12- and 20-μm diameter intermediate apertures and showing that the 285-eV signal is independent of aperture size. This indicates that the 285-eV signal does not arise from sampling of adjacent domains, at least for the micron scale domains detected in the X-PEEM images (vide infra).

3.2. Low molecular weight PS/PMMA thin films

The results for the high molecular weight PS/PMMA blends described above are difficult to reconcile with our earlier STXM studies of low MW PS/PMMA blends [16,17], which were interpreted in terms of complete phase segregation. One possible origin of different results is the large MW of the PS and PMMA components, as well as the difference in their values (1060K/312K) which may lead to differential mobility. It is likely the high MW systems are very far from thermodynamic equilibrium, even after annealing. In order to gain further insight into the origin of the PS signal in the surface region of the PMMA domains, which is clearly and consistently observed in NEXAFS recorded by X-PEEM, we have used X-PEEM, AFM and STXM to study a low molecular weight blend that has been more aggressively annealed than the 30/70 blend. The much lower molecular weight and the longer,

higher temperature anneal, should lead to a system much closer to equilibrium. In previous studies of 50:50 27K/27K PS/PMMA blends, Ade et al. [16] found via singular value decomposition (SVD) analysis of STXM micrographs that these systems have 'essentially pure domains' after rather short annealing times of 10 min at 180°C. Lateral force microscopy (also known as surface friction microscopy or SFM), providing frictional contrast, also showed that the 10-min annealed samples have a surface morphology that clearly matched that derived from NEXAFS microscopy [16]. However, the topography is smooth and on a much larger length scale, which supports the interpretation of the SFM as being due to differences in composition. To illustrate these findings, we show the SFM image in comparison to the PS, PMMA composition and total thickness maps derived from STXM of the 10-min annealed sample in Fig. 9. This study in particular did not detect PS in the PMMA matrix, except for small droplets. Furthermore, after 1 week of annealing a very different morphology was observed (Fig. 10). The STXM component maps as well as AFM imaging of the cyclohexane washed surface (which preferentially removes PS) clearly showed rims of PMMA around PS droplets sitting on top of a thin PMMA substrate-wetting layer. The height of the droplets was in excess of 500 nm, much larger than the original film thickness of 145 nm. The morphology of the droplets and the lack of significant further morphological evolution for longer anneal times indicated that morphologies close to the thermodynamic equilib-

rium had been reached; the larger PS domains slowly grow at the expense of the few remaining small PS domains via Ostwald ripening [1]. Further details of these results are given elsewhere [17]. The curvature of the PS phase at the air–PMMA–PS intersection at the PMMA rims (Fig. 10) would be difficult to explain if there were a PS surface layer on top of the PMMA matrix. The existence of the rim is a clear indication that the system attempts to balance the Newman equations at the interface [3].

Notwithstanding these unambiguous earlier results, we have investigated low molecular weight samples prepared similarly to the high MW films prepared for the preferential protein adsorption studies. To our surprise, X-PEEM showed that annealed low MW blends also have a PS signal at the surface of the PMMA-rich domains. X-PEEM results for an aggressively annealed 40/60 (wt.%/wt.%) PS/PMMA sample prepared from low molecular weight (21K/22K) components (see Table 1 for sample preparation details) are presented in Fig. 11. Fig. 11a and b shows PS and PMMA component maps derived from X-PEEM image sequence analysis. Spectral decomposition of the C 1s spectra extracted from the PS-rich (Fig. 11c) and PMMA-rich (Fig. 11d) regions are also indicated. These results indicate that: (a) lower molecular weight and more aggressive annealing gives rise to a more regular pattern of domains; (b) the PMMA phase forms the continuous matrix domain; and (c) the PS phase corresponds to elevated droplets. The latter two observations are particularly notable since they

| a | b | c | d |

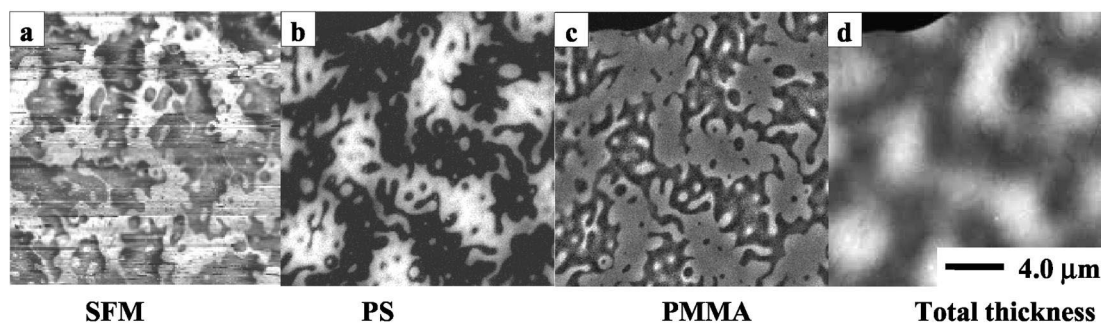**SFM**   **PS**   **PMMA**   **Total thickness**

Fig. 9. (a) Surface friction image (SFM); and (b) PS, (c) PMMA and (d) total thickness maps derived by SVD analysis of NEXAFS images recorded with STXM from a 50/50 w/w PS/PMMA (27K/27K) blend annealed for 10 min at 180°C. (NSLS STXM. Adapted from Ref. [16]).
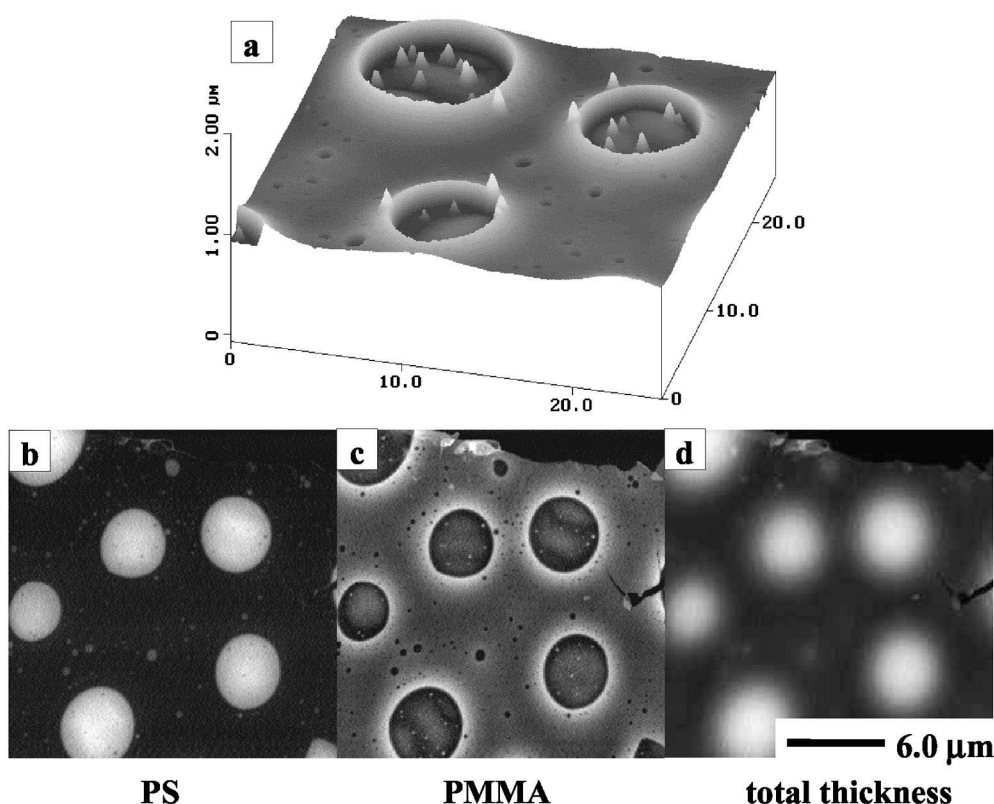
Fig. 10. Morphology of 50/50 w/w PS/PMMA (27K/27K) blend annealed for 1 week at 180°C. (a) AFM topography after preferential dissolution of PS via cyclohexane washing; (b) PS map, (c) PMMA map, (d) total thickness map derived from STXM. (NSLS STXM. Adapted from Ref. [16]).

are totally opposite to the situation with the 30/70 film made from the high MW components, where PS is the continuous phase (in the surface region at least) and it is the PMMA which forms protruding, elevated domains in the 30/70 film. The similarity of the samples shown in Fig. 11 to those in Fig. 10 led us to believe that equilibrium is essentially reached in the sample depicted in Fig. 11 as well. However a very large signal at 285 eV is observed in the NEXAFS of the surface region of the PMMA-rich matrix phase, as with the higher MW samples. Some of the 285-eV signal is associated with beam damage, since this particular data set was taken with too high incident flux, as indicated by the reduced height of the 288.4-eV signal relative to the C 1s continuum. Even so, a large proportion of the 285-eV signal is from PS in the near surface region of this sample.

This is fully confirmed by AFM of the annealed 40/60 low MW PS/PMMA sample after cyclohexane washing (Fig. 12a,b), which shows a bimodal distribution of PS domain sizes with the PMMA matrix containing a large number (~20%) of PS drops which are smaller than the X-PEEM resolution. Fig. 12c,d shows AFM of a 50/50 low MW PS/PMMA blend without the cyclohexane washing. In this case, the sample was annealed less aggressively and there are fewer of the small PS domains decorating the PMMA matrix.

We conclude that the 285.1-eV signal observed consistently in all X-PEEM studies of PS/PMMA blends arises from PS in the surface region, which AFM shows to be in the form of small PS droplets distributed on top of the surface of the PMMA domains. Since the earlier STXM studies [16,17] did
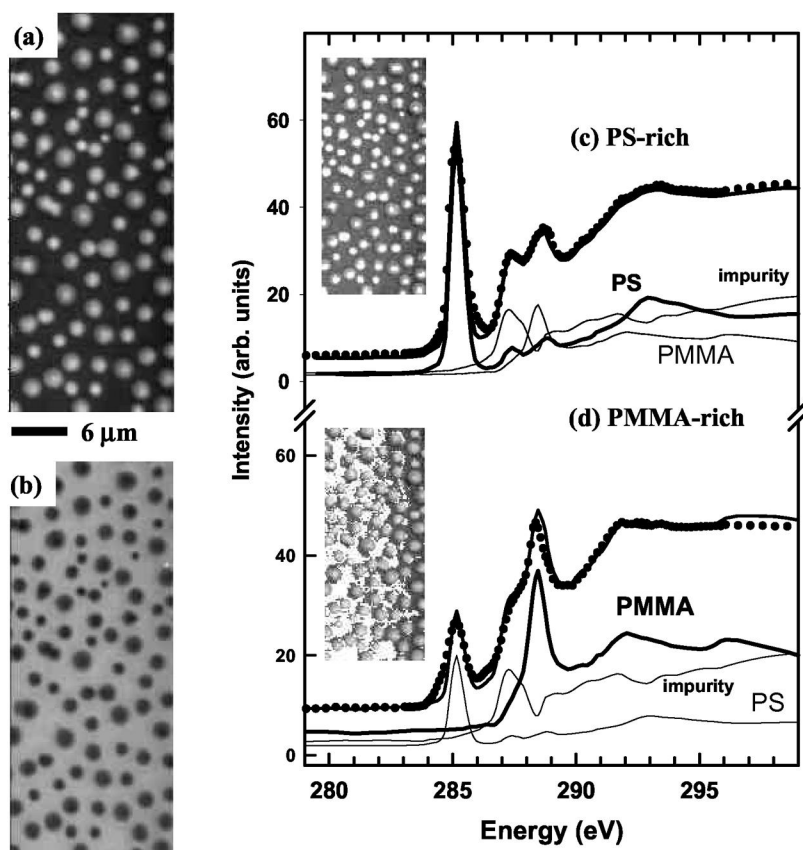
Fig. 11. (a) PS and (b) PMMA component maps derived from X-PEEM of an aggressively annealed low MW 50/50 PS/PMMA blend spun cast on a SiO$_x$ surface. Spectral decomposition of the C 1s spectra extracted from (c) the PMMA-rich (2.5*PS, 1.5*impurity, 0.2*PMMA) and (d) PS-rich (0.25*PS, 1.0*impurity, 1.8*PMMA) regions, at the locations indicated in the insert images (the reference spectra are edge jump-normalized). For this measurement the flux used was too high and the PMMA was damaged. However only part of the 285-eV signal in the PMMA-rich spectrum arises from beam damage, as can be seen by comparison to the C 1s spectrum of pure PMMA which has been radiation damaged to produce a similar level of reduction of the $\pi^*_{C=O}$ peak relative to the continuum. (ALS X-PEEM).

not explicitly test for the existence of a surface layer of PS, careful STXM measurements were carried out on the 40/60 low MW PS/PMMA sample. The 40/60 sample was floated from the Si substrate onto a TEM grid. The experiments were designed to minimize the radiation dose given to the samples to prevent the development of a potential 285-eV signal from damaged PMMA. Only two images where acquired: at 281.8 and 285.16 eV. The linear absorption coefficient for PMMA between these two energies is virtually unchanged, while that for PS changes dramatically. PS domains with a wide range

of size distribution were found with STXM. An example of these STXM results is shown in Fig. 13. Many small domains are observed at or below the spatial resolution limit of the X-PEEM. The composition of the PMMA matrix area between the small PS domains was carefully analyzed. The difference in the OD between the images acquired at the two energies in the PMMA region was less than 0.015. For PS, the difference in linear attenuation coefficient at these two energies is ~21 μm^{-1}. Hence, the upper limit for the thickness of a uniform PS layer would be 0.7 nm, even before taking into account
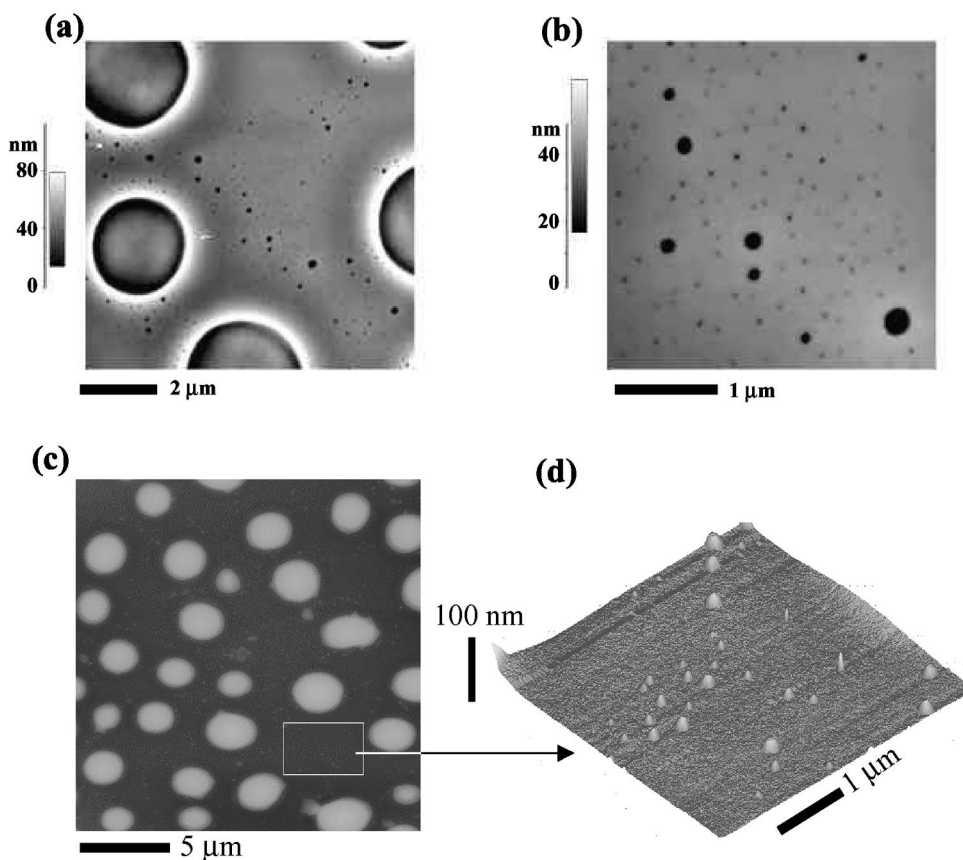
Fig. 12. (a) AFM image of the annealed low MW 50/50 PS/PMMA blend after washing with cyclohexane to remove surface PS. (b) Expanded region of the AFM shown in (a) which shows the pits where small droplets of PS have been removed (NCSU). (c) AFM (height mode) image of a 21K/21K 50/50 w/w PS/PMMA blend spun cast from toluene solution and vacuum annealed for 1 h at 180°C. (d) Expanded perspective view of the PMMA domain showing small PS droplets sitting on the surface (McMaster).

apparent signal due to the finite point spread function of the microscopy [30]. Assuming a sampling depth of 10 nm, a 0.7-nm overlayer would result in a smaller PS signal than that actually observed in X-PEEM. The PS signal seen in the PMMA regions with X-PEEM is thus attributed to small PS domains that can not be resolved in the X-PEEM results, which were recorded under conditions giving ∼200-nm spatial resolution. The high spatial resolution NSLS STXM study indicated that these small domains cover about a 20% area of the PMMA matrix in the 40/60 PS/PMMA sample, consistent with the AFM shown in Fig. 12a,b.

4. Discussion

The PS signal observed in the NEXAFS of the surface of the predominantly PMMA domains in all of the PS/PMMA blends is real. However we do not propose that this is experimental evidence that surface segregation to create a homogeneous PS layer on PMMA is thermodynamically preferred. Rather we attribute the signals to the existence of a bimodal size distribution for PS domains which includes a set of PS domains which are unresolved in X-PEEM. In the 40/60 and 50/50 low MW PS/ PMMA blend samples, AFM and STXM provided
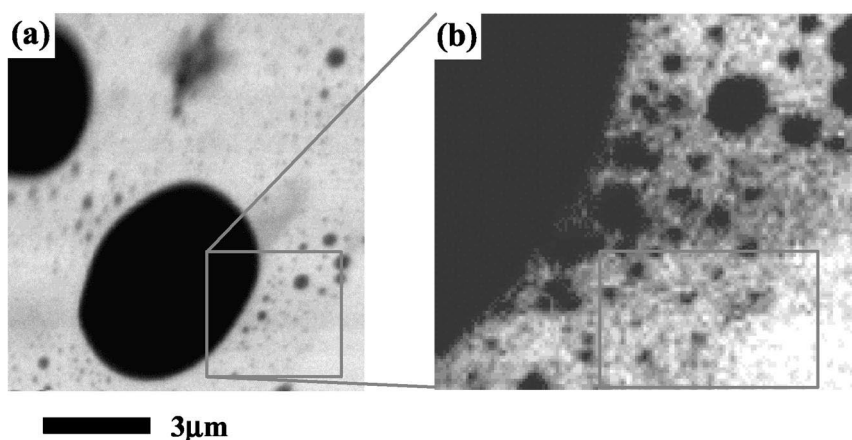
Fig. 13. (a) High resolution C 1s STXM image at 285.2 eV of 40/60 w/w PS/PMMA (21K/22K) blend annealed for 1 day at 165°C. (b) Expanded region of the STXM image shown in (a). Numerous small PS domains are readily visible. The area indicated in the lower part of (b) was used for the quantitative analysis discussed in the text. (NSLS STXM).

direct visualization of these micro domains, which persist due to the slow process of Ostwald ripening, even though these systems are relatively close to equilibrium. For the high MW 30/70 PS/PMMA blend, the system is likely still far from equilibrium, such that small PS domains initially formed at the surface of large PMMA domains have not been able to merge or ripen via diffusion with other PS regions to form a macro-domain.

The presence of small PS droplets in the PMMA domains and the deficit of PMMA in the AFM and X-PEEM of the 30/70 system, could be due to the generally low mobility of the large MW PS. Effectively the sample does not reach equilibrium under the annealing regime used. However it is surprising that the PS in the bulk of the sample has sufficient mobility to re-organize on micron length scales (compare Figs. 3 and 4) whereas the PS at the surface of the sample is immobile. One possible explanation is that when the PS-on-PMMA is in the form of very small isolated domains, they can not coalesce with other PS domains, but have to shrink via Ostwald ripening, i.e. diffusion, and thus overcome the repulsive interactions of the surrounding PMMA domain. In contrast, the large PS domains running through the whole film are areas where a continuous region of PS has initially formed and can rapidly coalesce.

For the 30/70 PS/PMMA system, the continuous regions of PS may arise because the PS comes out of solution more rapidly than PMMA on account of its higher MW (even though PS has a higher intrinsic solubility in toluene than PMMA does, for the same MW). If this is the case, then faster deposition of PS might lead to a structure in which there is a layer of PS near the substrate, with 'puddles' of PMMA embedded. This would explain why PS forms the continuous phase, even though it is the less abundant species. Finally, as indicated by the AFM (Figs. 3 and 4), there are a number of very fine PS domains in the large PMMA domains in the 30/70 sample. These are too small to detect by X-PEEM, but they would contribute to the spectrum.

There is clearly much more work to be done to understand and fully integrate the many aspects of this interesting polymer system, and to extend these results to the preparation of the surface differentiated PS/PMMA blend sample desired for competitive protein adsorption. Currently our strategy to achieve the latter is to use lower MW components (100K/100K), longer annealing (12 h or more at 140°C), and to improve our procedures to avoid impurity contamination. While clearly we would have preferred uncontaminated samples for this study, the detection and mapping of the impurity signal itself is a good example of how NEXAFS microscopy can

probe sample details missed by chemically insensitive probes such as AFM.

The large variety of morphologies and their different thermal evolution reported in the literature (as outlined in the Introduction) reflect the complexity of the PS/PMMA blend system which arises from a very fine balance of the forces controlling morphology and dynamics of phase segregation. We wish to emphasize the need for careful control of key parameters and a full reporting of the sample preparation, annealing and experimental measurements in order to facilitate cross-comparison of results. Further, examination of identical samples by complementary techniques should be used wherever possible.

The results reported here clearly demonstrate many ways in which both X-PEEM and STXM X-ray microscopy can be powerful tools for understanding phase segregation phenomena in blends and in other polymer systems. Although the current STXM and X-PEEM instruments have lower spatial resolution than AFM and TEM/SEM, they are a very useful complement to these higher resolution techniques because they provide direct chemical information. Finally, we note that soft X-ray microscopy can be applied to many problems other than phase segregation in polymers. Other recent studies of polymer properties include investigations of cross-link density in superabsorbent polymers [37], filler particles in polyurethanes [38], composition of core-shell micro-spheres [39], dewetting in PS-BrPS bilayer films [17,20], and pattern formation in free standing confined trilayer films [40].

References

[1] I.M. Campbell, Introduction To Synthetic Polymers, Oxford University Press, New York, 1994.

[2] S. Wu, J. Phys. Chem. 74 (1970) 632.

[3] S. Qu, C.J. Clarke, Y. Liu, M.H. Rafailovich, J. Sokolov, K.C. Phelan, G. Krausch, Macromolecules 30 (1997) 3640.

[4] T. Thurn-Albrecht, J. Schotter, C.A. Kastle, N. Emley, T. Shibauchi, L. Krusin-Elbaum, K. Guarini, C.T. Black, M.T. Tuominen, T.P. Russell, Science 290 (2000) 2126.

[5] S. Walheim, E. Schäffer, J. Mlynek, U. Steiner, Science 283 (1999) 520.

[6] J. Söhr, NEXAFS Spectroscopy, Series in Surface Science, Vol. 25, Springer, Berlin, 1992.

[7] K. Dalnoki-Veress, J.A. Forrest, J.R. Stevens, J.R. Dutcher, Physica A 239 (1997) 87.

[8] K. Tanaka, K. Takahara, T. Kajiyama, Macromolecules 29 (1999) 3232.

[9] S. Walheim, M. Boltau, J. Mlynek, G. Krausch, U. Steiner, Macromolecules 30 (1997) 4995.

[10] D.A. Winesett, S. Zhu, J. Sokolov, M. Rafailovitch, H. Ade, J. High Perf. Polymers 49 (2000) 458.

[11] C. Thon-That, A.G. Shard, R. Dalay, R.H. Bradley, Macroelcules 33 (2000) 8453.

[12] C. Thon-That, A.G. Shard, D.O.H. Teare, R.H. Bradley, Polymer 42 (2001) 1121.

[13] D. Slep, J. Asselta, M.H. Rafailovich, J. Sokolov, D.A. Winesett, A.P. Smith, H. Ade, S. Anders, Langmuir 16 (2000) 2369.

[14] P. Mansky, Y. Liu, E. Huang, T.P. Russell, C. Hawker, Science 275 (1997) 1458.

[15] E. Kumacheva, L. Li, M.A. Winnik, D.M. Shinozaki, P.C. Cheng, Langmuir 13 (1997) 2483.

[16] H. Ade, D.A. Winesett, A.P. Smith, S. Qu, S. Ge, J. Sokolov, M. Rafailovich, Europhys. Lett. 45 (1999) 526.

[17] H. Ade, D.A. Winesett, A.P. Smith, S. Anders, T. Stammler, C. Heske, D. Slep, M.H. Rafailovich, J. Sokolov, J. Stohr, Appl. Phys. Lett. 73 (1998) 3775.

[18] A. Karim, T.M. Slawecki, S.K. Kumar, J.F. Douglas, S. Satija, C.C. Han, T.P. Russell, Y. Liu, R. Overney, J. Sokolov, M.H. Rafailovich, Macromolecules 31 (1998) 857.

[19] T. Schmitt, P. Guttmann, O. Schmidt, P. Müller-Buschbaum, M. Stamm, G. Schönhense, G. Schmahl, X-ray Microscopy, AIP Conf. Proc 507 (2000) 245, editors: W. Meyer Ilse, T. Warwick and D. Attwood.

[20] D. Slep, J. Asselta, M.H. Rafailovich, J. Sokolov, D.A. Winesett, A.P. Smith, H. Ade, Y. Strzhemechny, S.A. Schwarz, B.B. Sauer, Langmuir 14 (1998) 4860.

[21] J. Kirz, C. Jacobsen, M. Howells, Q. Rev. Biophys. 28 (1995) 33.

[22] H. Ade, in: J.A.R. Samson, D.L. Ederer (Eds.), Experimental Methods in the Physical Sciences, Vol. 32, Academic Press, New York, 1998, p. 225.

[23] H. Ade, S.G. Urquhart, in: T.K. Sham (Ed.), Chemical Applications of Synchrotron Radiation, World Scientific Publishing, Singapore, 2000 (in press).

[24] C. Jacobsen, S. Wirick, G. Flynn, C. Zimba, J. Microsc. 197 (2000) 173.

[25] I.N. Koprinarov, A.P. Hitchcock, C.T. McCrory, R.F. Childs, J. Phys. Chem. B (submitted).

[26] A.P. Hitchcock, I.N. Koprinarov, H. Stöver, L. Croll, E. Kneedler (in preparation).

[27] A.P. Hitchcock, I.N. Koprinarov, T. Tyliszczak, C. Morin, Y.M. Heng, R. Cornelius, J.L. Brash, H. Ade, S. Anders, A. Scholl, F. Notling, ALS Compendium, 2000, LBNL publication, 47838.

[28] T. Warwick, K. Franck, J.B. Kortwight, G. Meigs, M. Moronne, S. Myneni, E. Rotenberg, S. Seal, W.F. Steele, H. Ade, A. Garcia, S. Cerasari, J. Denlinger, S. Hayakawa, A.P. Hitchcock, T. Tyliszczak, E.G. Rightor, H.-J. Shin, B. Tonner, Rev. Sci. Inst. 69 (1998) 2964.

[29] C. Jacobsen, H. Ade, J. Kirz, C.-H. Ko, S. Williams, X. Zhang, E. Anderson, D. Kern, Scanning soft X-ray microscopy, in (Eds.) P.B. Kenway, P.J. Duke, G.W. Lorimer, T. Mulvey, I.W. Drummond, G. Love, A.G. Michette, M. Stedman, X-ray Optics and Microanalysis 1992. Bristol, 10P Publishing, 571.

[30] D. Sayre, H.N. Chapman, Acta Crystallogr. A51 (1995) 237.

[31] M. Feser, M. Carlucci-Dayton, C. Jacobsen, J. Kirz, U. Neuhäusler, G. Smith, B. Yu, X-ray Microfocusing: Applications and Techniques, I. McNulty (Ed.), SPIE Proc. 3449 (1998) 19.

[32] B.L. Henke, P. Lee, T.J. Tanaka, R.L. Shimabukuro, B.K. Fujikawa, At. Nucl. Data Tables 27 (1982) 1.

[33] J. Brandrup, E.H. Immergut, E.A. Grulke (Eds.), Polymer Handbook, 4th Edition, Wiley, 1999.

[34] S. Anders, H.A. Padmore, R.M. Duarte, T. Renner, T. Stammler, A. Scholl, M.R. Scheinfein, J. Stöhr, L. Séve, B. Sinkovic, Rev. Sci. Inst. 70 (1999) 3973.

[35] Y. Wang, C. Jacobsen, J. Maser, A. Osanna, J. Microsc. 197 (2000) 80.

[36] T. Coffey, S.G. Urquhart, H. Ade, J. Electron Spectrosc. (in press).

[37] G.E. Mitchell, L.R. Wilson, M.T. Dineen, S.G. Urquhart, F. Hayes, E.G. Rightor, A.P. Hitchcock, H. Ade, Macromolecules (in press).

[38] A.P. Hitchcock, J. Koprinarov, T. Tyliszczak, E.G. Rightor, G.E. Mitchell, M.T. Dineen, F. Hayes, W. Lidy, R.D. Priester, S.G. Urquhart, A.P. Smith, H. Ade, Ultramicroscopy 88 (2001) 33.

[39] I.N. Koprinarov, A.P. Hitchcock, W.H. Li, Y.M. Heng, H.D.H. Stöver, Macromolecules 34 (2001) 4424.

[40] I.N. Koprinarov, A.P. Hitchcock, K. Dalnoki-Varess, C. Murray, J. Dutcher, H. Ade, J. Phys. B (in preparation).